Fabrication of large-area 3D optical fishnet metamaterial by laser interference lithography

Y. Zhou, X. Y. Chen, Y. H. Fu, G. Vienne, A. I. Kuznetsov et al.

Citation: Appl. Phys. Lett. **103**, 123116 (2013); doi: 10.1063/1.4821508
View online: http://dx.doi.org/10.1063/1.4821508
View Table of Contents: http://apl.aip.org/resource/1/APPLAB/v103/i12
Published by the AIP Publishing LLC.

Fabrication of large-area 3D optical fishnet metamaterial by laser interference lithography

Y. Zhou,[a] X. Y. Chen, Y. H. Fu, G. Vienne, A. I. Kuznetsov, and B. Luk'yanchuk
*Data Storage Institute, A*STAR (Agency for Science, Technology and Research), DSI Building, 5 Engineering Drive 1, Singapore 117608*

(Received 17 June 2013; accepted 2 September 2013; published online 20 September 2013)

Centimeter-scale 3D fishnet metamaterial with negative refractive index in the near infrared spectral range is demonstrated. The large-area fabrication is realized using a conventional laser interference lithography technique in combination with a tri-layer lift-off procedure. This method allows us to effectively achieve a centimeter-scale 3D fishnet structure with a pitch of 600 nm and five functional Ag/SiO_2 bi-layers with a total thickness of 300 nm. The experimental transmission spectrum correlates well with simulation results. Effective refractive index versus frequency associated with permittivity and permeability are retrieved. Two negative refractive index regions are found in the near-infrared spectral range. © *2013 AIP Publishing LLC*. [http://dx.doi.org/10.1063/1.4821508]

Metamaterials attract growing interest of researches due to their unique properties which do not exist in nature.[1–10] The fishnet structure is one of the best known metamaterial designs, which allows realizing negative refractive index at optical frequencies. The unit cells of a fishnet metamaterial consist of cut-wire pairs exhibiting magnetic resonant response, which can lead to a negative magnetic permeability, and continuous metallic strips exhibiting negative electric permittivity.[11–14] Varying dimensions, periodicity, and materials, the fishnet structure can obtain negative refractive index in the mid-IR and near-IR spectral range.[11–15] Increasing the number of functional layers of a fishnet structure, a strong magneto-inductive coupling can be generated between adjacent layers. It leads to a broadband (1.75 μm–2.4 μm) negative refractive index with high figure of merit (FOM) ($\sim$3.5).[14,16] Technologies reported for fabrication of fishnet metamaterials so far can be divided into 2 categories: patterning-first processes and multi-layer film deposition-first processes. The former includes multi-layer electron beam lithography (EBL),[15] nanoimprint,[14] or interference lithography (IL).[7] The latter mainly refers to the use of focused ion beam (FIB).[13] Single-beam processes, like FIB or EBL, have a low speed which limits their applications to large-area structure fabrication. However, these methods can provide excellent control over feature sizes. Even though the layer-by-layer EBL technique can be seen as a general method for fabrication of 3D metamaterials, it requires additional planarization techniques and careful lateral alignment of different layers.[15] Nanoimprint and various forms of soft lithography, although readily applicable to 3D structure fabrication, are complicated due to challenges in the lift-off process.[14,17] To increase the probability of successful lift-off, the thickness of multi-stack film should be less than 50% of the thickness of the sacrificial layer, which is determined by the patterning techniques.

In this paper, we introduce a method for fishnet metamaterial fabrication which combines a tri-layer lift-off process to obtain a 3D multi-layer structure with the laser interference lithography (LIL) to obtain centimetre-scale patterning. We employ Lloyd's LIL setup, which allows to fabricate submicron periodic patterns with a flexible control over line and space widths. Usually, LIL can only be used to fabricate patterns with <1 aspect ratio due to depth-dependent absorption and intrinsic sinusoidal interference wave property: the profile tends to be tapered around 35°. Such a tapered profile is not suitable for subsequent lift-off process. In our study, LIL was only used for patterning of a top resist layer, while another tri-layer lift-off process was developed to transfer pillars into a sacrificial layer with >5 aspect ratio. This allowed us to realize a 5-bi-layer metamaterial with the thickness of multi-stack film of around 300 nm. This cannot be achieved by standard LIL process.

Figure 1 shows the developed fabrication procedure. Silicon was selected as a substrate considering that it is transparent in the near-infrared spectral range. The silicon substrate was first spin coated with $\sim$1 μm sacrificial layer of S1805 photoresist (Rohm and Haas) followed by sputtering of a 50 nm SiO_2 hard mask layer and deposition of another thin imaging layer of S1805 photoresist. The sample was then exposed twice under a 325 nm Lloyd's laser interference lithography setup with 90° rotation applied after the first exposure (Fig. 1(b)). The pitch was tuned to be of 600 nm by adjusting the angle of incidence to 15.5°. After developing the top photoresist layer, pillar arrays were achieved (Fig. 1(c)). Then reactive ion etching (RIE) was used to open the SiO_2 hard mask with CF_4 gas (Fig. 1(d)). Subsequently, O_2 plasma was used to etch the bottom 1 μm thick photoresist layer (Fig. 1(e)). Since SiO_2 has no reaction with O_2 plasma, the selectivity can be very high. This high selectivity provided the possibility to form >5 aspect ratio pillars with slightly undercut profile as shown by the SEM image in Fig. 2(a). Apart from photoresist, different organic films can be used as sacrificial layers as long as they can be etched with O_2 plasma. The undercut, which is critical for the lift-off process, is also tunable by adjusting the O_2 flow and the chamber pressure. Five alternating Ag/SiO_2 bi-layers with thickness of 30/30 nm each were then deposited by e-beam evaporation (Fig. 1(f)). To protect the last Ag layer from oxidation, a SiO_2 layer was coated on top. The deposited sample was then immersed into PG Remover (MicroChem). Photoresist pillars dissolved in the remover

[a]Electronic mail: Zhou_yi@dsi.a-star.edu.sg

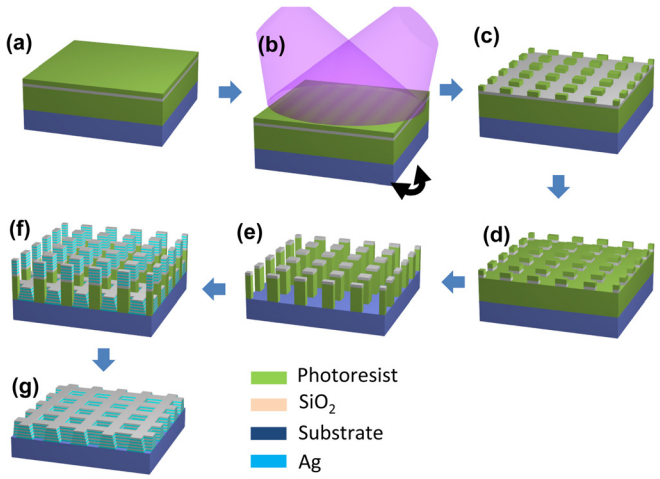

FIG. 1. Schematic of the combined laser interference lithography and tri-layer lift-off process for large-area 3D fishnet metamaterial fabrication: (a) tri-layer system consisting of a sacrificial photoresist, SiO_2 hard mask, and imaging photoresist layers; (b) large area pattering of the imaging photoresist layer by double-exposure laser interference lithography; (c) photoresist pillar array after the development process; (d) opening of the SiO_2 hard mask layer by RIE with CF_4 plasma; (e) O_2 plasma etching of the sacrificial photoresist layer forming >5 aspect ratio pillars due to very high etching selectivity; (f) deposition of dielectric and metallic multilayer thin films; (g) lift-off of the sacrificial photoresist pillars to form the 3D fishnet metamaterial.

leaving a fishnet structure with 5 functional bi-layers behind (Fig. 1(g)).

Figure 2(b) shows images of the fabricated large-area 3D fishnet metamaterial. The inserted photograph demonstrates that around 1 cm^2 area structure was fabricated. The UV laser power used for this process was 14 mW. Larger area patterning can be achieved with a higher power laser. Figure 2(c) shows a cross-sectional SEM image of the fabricated 3D metamaterial with five alternative Ag/SiO_2 bi-layers. Because of the deposition step coverage effect, the profile of the holes has a trapezoidal rather than a rectangular shape, the side wall angle being around 70°. The pitch of the structure is 600 nm and the hole diameters on the bottom and top layers are 305 nm and 525 nm, respectively. The smallest achievable pitch is dependent on the laser source wavelength

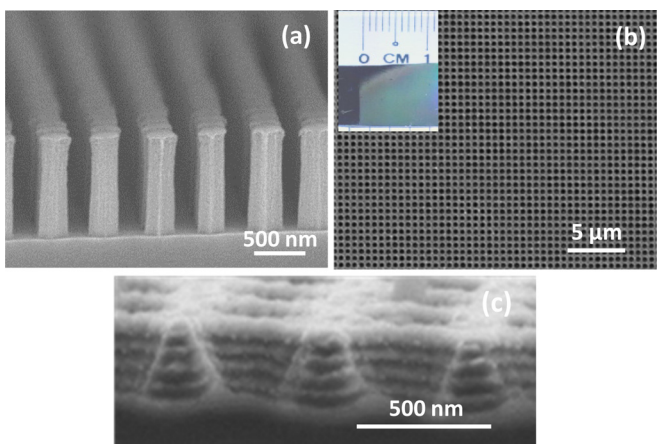

FIG. 2. (a) Cross-sectional SEM image of the high aspect ratio (~5) photoresist pillar array with slightly undercut profile after O_2 plasma etching; (b) Top view SEM image of the fabricated 3D fishnet metamaterial, with a period of 600 nm. Inset is a large-area optical image showing a >1 cm^2 patterned area (c) Cross-sectional SEM image of the fishnet structure with 5 Ag/SiO_2 bi-layers each of 30/30 nm thickness.

and the angle of incidence. Practically, it is around the laser wavelength. The film thickness for each layer is around 30 nm and the total structure has a thickness of about 300 nm, which is a very high value compared to all lift-off fabricated fishnet metamaterials reported so far.[7,18–20]

To characterize optical properties of the fabricated fishnet metamaterial, we measured the transmission spectrum of the structure using a commercial UV-Vis-IR spectrophotometer (UV3600, SHIMADZU). The spectrum was collected from a large area with a beam diameter of around 2 mm in the near infrared spectral range. The experimental transmittance spectrum is shown by the black curve in Fig. 3(a). The measured spectral shape is comparable with spectra of fishnet structures reported in previous publications.[7,15,18]

A finite-difference time-domain (FDTD) software (Lumerical FDTD Solutions) was used to simulate optical properties of the fabricated fishnet metamaterial and retrieve effective parameters. The simulated transmission spectrum is shown by the red curve in Fig. 3(a). Experimental parameters of the real fishnet structure extracted from SEM images in Figs. 2(b) and 2(c) were used for building the FDTD model. The permittivity of silver was described by the Drude model[21] with the plasma frequency $\omega_p = 1.37 \times 10^{16}$ s^{-1} and the damping constant $\gamma = 1.6 \times 10^{14}$ s^{-1}. To account for both interface roughness and tapered side wall scattering, the value of γ was multiplied by a factor of 6. The simulation result shows a good agreement with the experiment, which allows for further theoretical analysis of the metamaterial properties.

The effective refractive index versus frequency retrieved from FDTD simulations is presented in Fig. 3(b). In previous studies of similar fishnet structures, only a single negative effective refractive index region close to ω_3 was found.[13,22]

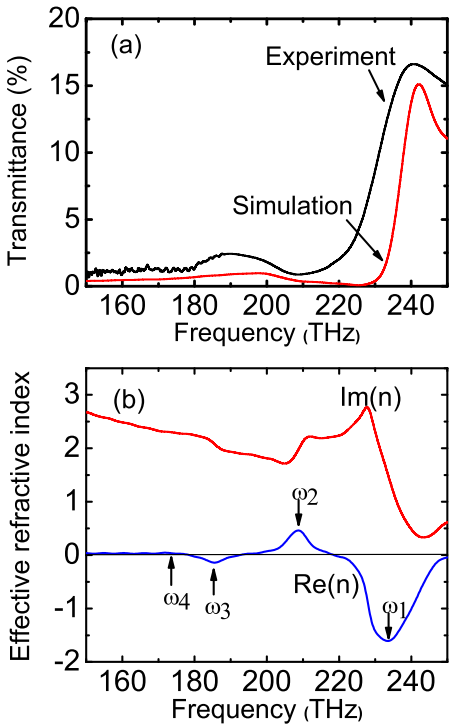

FIG. 3. (a) Experimental and simulated transmittance spectra of the fabricated fishnet structure in the near infrared spectral range; (b) Effective refractive index retrieved using FDTD software with experimental geometrical dimensions.

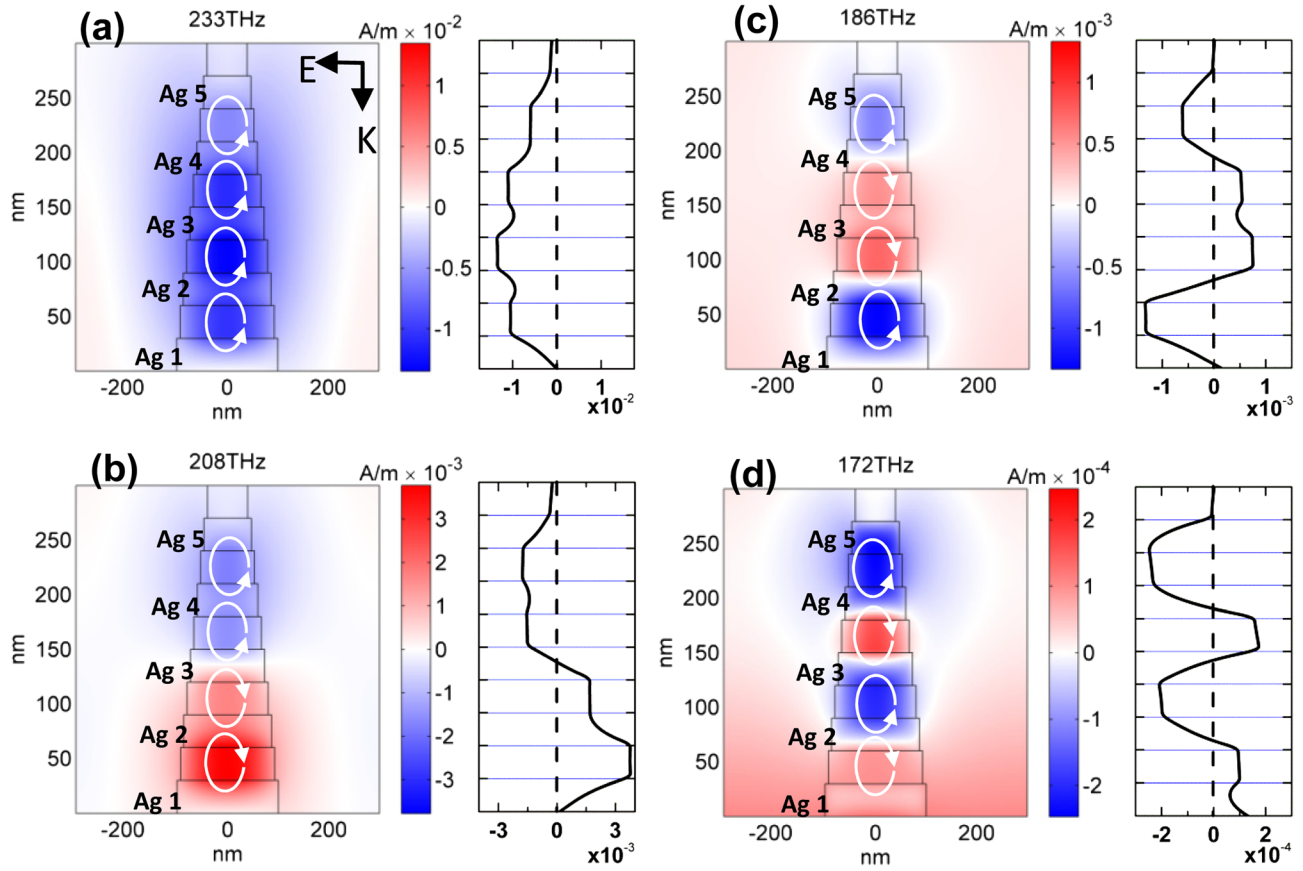

FIG. 4. Magnetic field distribution at 4 resonance frequencies: (a) $\omega_1 = 233$ THz; (b) $\omega_2 = 208$ THz; (c) $\omega_3 = 186$ THz; (d) $\omega_4 = 172$ THz, in each unit cell of the simulated fishnet structure. For clarity, Ag layers are marked with consequential numbers in each figure. White arrows indicate the direction of displacement currents. Right panels show the magnetic field profile at each resonant frequency.

In our case, however, the second negative index range is observed at a higher frequency ω_1. We attribute the appearance of this region to high-order Bloch modes. Due to the excitation and coupling of high-order Bloch modes, whose amplitudes may exceed the one of the fundamental mode, the retrieval algorithm is not valid for effective refractive index. Therefore, the retrieved effective index curve is non-convergent with increasing frequency.[15,22,23] Since the structure profile in our case is tapered and the top layer width (75 nm) is smaller than the bottom layer (295 nm), the high-order Bloch mode coupling with neighboring unit cells is significantly weakened. This increases losses of the high-order Bloch modes and reduces their influence in the higher frequency range. Subsequently, the effective refractive index in this range becomes convergent and two additional extrema at frequencies ω_1 and ω_2 can be found.

To better understand the nature of the main resonances observed in the effective refractive index curve (Fig. 3(b)), in Figs. 4(a)–4(d) we plot the magnetic field distribution at the three resonant frequencies (233 THz, 208 THz, and 186 THz). Magnetic dipole resonances are observed and these resonances are excited due to the displacement current loops confined inside the dielectric layers between neighboring Ag layers. Both in-phase and out-of-phase resonances can be detected. The in-phase resonances (red color) strengthen the external magnetic field while the out-of-phase resonances (blue color) weaken the external magnetic field, which lowers the magnetic permeability and can lead to a negative refractive index. For the magnetic oscillation mode at $\omega_1 = 233$ THz, all dipoles are opposite to the external magnetic field so that the external field is weakened significantly resulting in a value of -1.5 for the refractive index. For the mode at $\omega_2 = 208$ THz, 2 in-phase and 2 out-of-phase resonances are confined in different dielectric layers. In the far field zone, the opposite-sign resonances in neighboring layers cancel each other. Therefore, the resulting oscillation is in-phase leading to a positive refractive index. Similarly for the mode at $\omega_3 = 186.3$ THz, 2 out-of-phase and 2 in-phase resonances generate a weak out-of-phase oscillation, which contributes to the 2nd negative refractive index region. Since the intensity of H here is one order of magnitude smaller than that at ω_1, the effective refractive index is only slightly less than 0. For a fishnet metamaterial with 5 functional layers, 4 resonant modes are expected. In our case, the 4th resonance at ω_4 is almost invisible. The magnetic field at this frequency is plotted in Fig. 4(d). Two in-phase and two out-of-phase magnetic resonances can be observed. Totally, the sum of these oscillations is close to 0 due to the anti-symmetric geometry. Furthermore, the amplitude of the field at ω_4 is 100 times smaller than that at ω_1. The four resonant modes described above are very similar to results discussed in Ref. 13. The only difference is in the resonance shapes, which can be attributed to the tapered profiles of the holes in our structure.

Finally in Fig. 5(a), we plot the FOM of the fabricated fishnet metamaterial. It is calculated as the ratio of the real

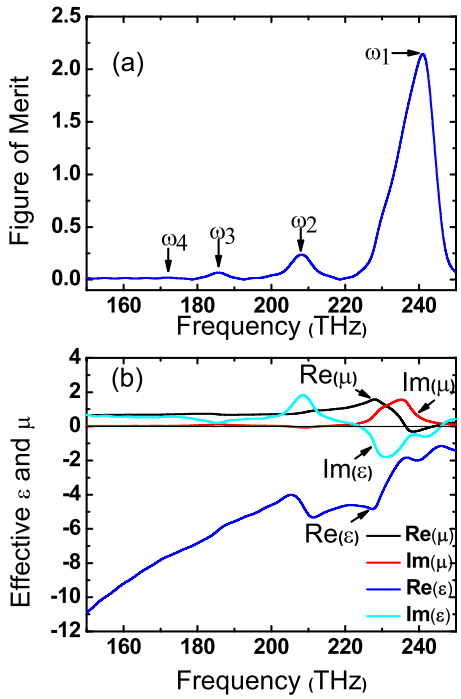

FIG. 5. Figure of merit (a) and complex permittivity and permeability (b) retrieved using FDTD software for a fishnet metamaterial with parameters corresponding to the experimental structure.

part to imaginary part of the refractive index [$|Re(n)/Im(n)|$]. Four FOM peaks are marked accordingly in Fig. 5(a). Fig. 5(b) shows the effective permittivity and permeability retrieved from the calculations. It is clearly seen that the real part of the magnetic permeability is only negative around 235 THz. Therefore, in this spectral range, the structure becomes a so called double-negative metamaterial with the FOM of 2.3. At other resonant wavelengths, $\mathrm{Re}(\mu) > 0$ and the FOMs are close to 0.

In conclusion, a centimeter-scale 5 bi-layer fishnet metamaterial with a pitch of 600 nm and a total thickness of 300 nm was fabricated by a combination of laser interference lithography and tri-layer lift-off techniques. The structure was analyzed through optical transmission measurements and simulated using FDTD software. Two negative refractive index regions were found in the near-infrared spectral range. Apart from the first negative-index range at around 190 THz, which is typical for fishnet structures, a second region was found at higher frequency around 230 THz. Appearance of this range was explained by the trapezoidal cross-section of the fishnet holes, which weaken higher-order Bloch modes.

This work was supported by the Agency for Science Technology and Research under SERC Grant No. 0921540099.

[1]V. M. Shalaev, Nat. Photonics **1**, 41 (2007).
[2]J. B. Pendry, A. J. Holden, D. J. Robbins, and W. J. Stewart, IEEE Trans. Microwave Theory Tech. **47**, 2075 (1999).
[3]J. B. Pendry, Phys. Rev. Lett. **85**, 3966 (2000).
[4]R. A. Shelby, D. R. Smith, and S. Schultz, Science **292**, 77 (2001).
[5]S. Linden, C. Enkrich, M. Wegener, J. F. Zhou, T. Koschny, and C. M. Soukoulis, Science **306**, 1351 (2004).
[6]G. Dolling, C. Enkrich, M. Wegener, J. F. Zhou, C. M. Soukoulis, and S. Linden, Opt. Lett. **30**, 3198 (2005).
[7]S. Zhang, W. J. Fan, N. C. Panoiu, K. J. Malloy, R. M. Osgood, and S. R. J. Brueck, Phys. Rev. Lett. **95**, 137404 (2005).
[8]W. S. Cai, U. K. Chettiar, H. K. Yuan, V. C. de Silva, A. V. Kildishev, V. P. Drachev, and V. M. Shalaev, Opt. Express **15**, 3333 (2007).
[9]C. M. Soukoulis and M. Wegener, Nat. Photonics **5**, 523 (2011).
[10]N. I. Zheludev, Science **328**, 582 (2010).
[11]G. Dolling, C. Enkrich, M. Wegener, C. M. Soukoulis, and S. Linden, Science **312**, 892 (2006).
[12]A. Boltasseva and V. M. Shalaev, Metamaterials **2**, 1 (2008).
[13]J. Valentine, S. Zhang, T. Zentgraf, E. U. Avila, D. A. Genov, G. Bartal, and X. Zhang, Nature **455**, 376 (2008).
[14]D. Chanda, K. Shigeta, S. Gupta, T. Cain, A. Carlson, A. Mihi, A. J. Baca, G. R. Bogart, P. Braun, and J. A. Rogers, Nat. Nanotechnol. **6**, 402 (2011).
[15]N. Liu, L. W. Fu, S. Kaiser, H. Schweizer, and H. Giessen, Adv. Mater. **20**, 3859 (2008).
[16]G. V. Eleftheriades, IEEE Microw. Wirel. Compon. Lett. **17**, 412 (2007).
[17]N. Kehagias, V. Reboud, G. Chansin, M. Zelsmann, C. Jeppesen, C. Schuster, M. Kubenz, F. Reuther, G. Gruetzner, and C. M. S. Torres, Nanotechnology **18**, 175303 (2007).
[18]G. Dolling, M. Wegener, C. M. Soukoulis, and S. Linden, Opt. Lett. **32**, 53 (2007).
[19]V. M. Shalaev, W. Cai, U. K. Chettiar, H. K. Yuan, A. K. Sarychev, V. P. Drachev, and A. V. Kildishev, Opt. Lett. **30**, 3356 (2005).
[20]K. Lodewijks, N. Verellen, W. V. Roy, V. Moshchalkov, G. Borghs, and P. V. Dorpe, Appl. Phys. Lett. **98**, 091101 (2011).
[21]P. B. Johnson and R. W. Christy, Phys. Rev. B **6**, 4370 (1972).
[22]C. Rockstuhl, T. Paul, F. Lederer, T. Pertsch, T. Zentgraf, T. P. Meyrath, and H. Giessen, Phys. Rev. B **77**, 035126 (2008).
[23]Q. Z. Li, W. H. Lin, and G. P. Wang, Appl. Phys. Lett. **99**, 041109 (2011).